AIP Journal of Applied Physics

Atomic layer deposition of crystalline SrHfO3 directly on Ge (001) for high-k dielectric applications

Martin D. McDaniel, Chengqing Hu, Sirong Lu, Thong Q. Ngo, Agham Posadas, Aiting Jiang, David J. Smith, Edward T. Yu, Alexander A. Demkov, and John G. Ekerdt

Citation: Journal of Applied Physics **117**, 054101 (2015); doi: 10.1063/1.4906953
View online: http://dx.doi.org/10.1063/1.4906953
View Table of Contents: http://scitation.aip.org/content/aip/journal/jap/117/5?ver=pdfcov
Published by the AIP Publishing

Articles you may be interested in

Accurate characterization and understanding of interface trap density trends between atomic layer deposited dielectrics and AlGaN/GaN with bonding constraint theory
Appl. Phys. Lett. **106**, 243503 (2015); 10.1063/1.4922799

Improved thermal stability and electrical properties of atomic layer deposited HfO2/AlN high-k gate dielectric stacks on GaAs
J. Vac. Sci. Technol. A **33**, 01A136 (2015); 10.1116/1.4903367

Atomic layer deposition of La x Zr 1 − x O 2 − δ (x = 0.25) high- k dielectrics for advanced gate stacks
Appl. Phys. Lett. **94**, 053504 (2009); 10.1063/1.3075609

Suppressed growth of unstable low- k Ge O x interlayer in Ge metal-oxide-semiconductor capacitor with high- k gate dielectric by annealing in water vapor
Appl. Phys. Lett. **90**, 163502 (2007); 10.1063/1.2723074

Atomic layer deposition of gadolinium scandate films with high dielectric constant and low leakage current
Appl. Phys. Lett. **89**, 133512 (2006); 10.1063/1.2354423

Goodfellow
metals • ceramics • polymers
composites • compounds • glasses
Save 5% • Buy online
70,000 products • Fast shipping

[This article is copyrighted as indicated in the article. Reuse of AIP content is subject to the terms at: http://scitation.aip.org/termsconditions. Downloaded to] IP: 149.169.223.129 On: Thu, 22 Oct 2015 20:07:53

CrossMark

Atomic layer deposition of crystalline $SrHfO_3$ directly on Ge (001) for high-*k* dielectric applications

Martin D. McDaniel,[1] Chengqing Hu,[2] Sirong Lu,[3] Thong Q. Ngo,[1] Agham Posadas,[4] Aiting Jiang,[2] David J. Smith,[3] Edward T. Yu,[2] Alexander A. Demkov,[4] and John G. Ekerdt[1,a)]

[1]*Department of Chemical Engineering, The University of Texas at Austin, Austin, Texas 78712, USA*
[2]*Microelectronics Research Center, The University of Texas at Austin, Austin, Texas 78758, USA*
[3]*Department of Physics, Arizona State University, Tempe, Arizona 85287, USA*
[4]*Department of Physics, The University of Texas at Austin, Austin, Texas 78712, USA*

(Received 9 October 2014; accepted 17 January 2015; published online 3 February 2015)

The current work explores the crystalline perovskite oxide, strontium hafnate, as a potential high-*k* gate dielectric for Ge-based transistors. $SrHfO_3$ (SHO) is grown directly on Ge by atomic layer deposition and becomes crystalline with epitaxial registry after post-deposition vacuum annealing at $\sim$700 °C for 5 min. The 2×1 reconstructed, clean Ge (001) surface is a necessary template to achieve crystalline films upon annealing. The SHO films exhibit excellent crystallinity, as shown by x-ray diffraction and transmission electron microscopy. The SHO films have favorable electronic properties for consideration as a high-*k* gate dielectric on Ge, with satisfactory band offsets (>2 eV), low leakage current ($<10^{-5}$ A/cm^2 at an applied field of 1 MV/cm) at an equivalent oxide thickness of 1 nm, and a reasonable dielectric constant ($k \sim 18$). The interface trap density (D_{it}) is estimated to be as low as $\sim 2 \times 10^{12}$ cm^{-2}eV^{-1} under the current growth and anneal conditions. Some interfacial reaction is observed between SHO and Ge at temperatures above $\sim$650 °C, which may contribute to increased D_{it} value. This study confirms the potential for crystalline oxides grown directly on Ge by atomic layer deposition for advanced electronic applications. © *2015 AIP Publishing LLC*. [http://dx.doi.org/10.1063/1.4906953]

I. INTRODUCTION

In the last decade, significant material changes to complementary metal oxide semiconductor (CMOS) devices have included the introduction of strained Si channels to improve performance and efficiency and metal gate/high-*k* dielectric stacks to address leakage current issues.[1–3] More recently, there has been renewed interest in using Ge as a channel material due to its higher hole (1900 vs. 500 cm^2/V s) and electron (3900 vs. 1400 cm^2/V s) mobility compared to Si.[4–7] Crystalline oxides are also being considered by the semiconductor industry as next-generation high-*k* dielectrics.[8] For example, there is tremendous interest in epitaxial integration of perovskite oxides, such as $SrTiO_3$ (STO) or $BaTiO_3$ (BTO), on semiconductors due to their functional properties and very high permittivities.[9–12] One primary advantage of crystalline, epitaxial dielectrics is the possibility of having virtually no defects in the bulk of the dielectric or at the interface with the semiconductor in an ideal heteroepitaxial system. For practical realization of high-mobility channels in CMOS technology, surface passivation of the semiconductor substrate and a high-quality oxide-semiconductor interface must be realized.

Integration of high-*k* dielectrics on germanium has been studied by many groups,[13–19] but the electrical performance of Ge-based devices has been less than optimal. Several methods have been employed to control the interface trap density (D_{it}) in order to achieve high performance.[15,16,18] Typical values reported for high-*k*/Ge gate stacks show $D_{it} \sim 10^{11}$–10^{12} cm^{-2}eV^{-1}. However, crystalline oxides have the potential to create a nearly perfect electrical interface by drastically reducing the interface trap density ($D_{it} < 10^{10}$ cm^{-2}eV^{-1}).[19,20] For a material to be suitable as a gate dielectric replacement, it needs to satisfy several requirements, including high permittivity, sufficiently large band gap and proper band alignment (with 1 eV offset to both bands) to the semiconductor, thermodynamic stability, good film morphology, and high interface quality. Materials related to TiO_2, including STO and BTO, have high permittivities, but the conduction band offsets with Si and Ge are very small to negligible.[21–23] Alternatively, crystalline strontium hafnate, $SrHfO_3$ (SHO), meets many of the high-*k* requirements and has a reasonable lattice match to Ge ($\sim$1.9% mismatch), making it an ideal material candidate for Ge-based transistors.

There are relatively few reports on thin film deposition of SHO to date.[24–32] In some early work, crystalline SHO was investigated as a future gate dielectric material for Si-based devices.[25,27] The SHO films were grown by molecular beam epitaxy (MBE) on Si (001) despite the 6% lattice mismatch. The electrical performance of epitaxial SHO on Si showed low equivalent oxide thickness (EOT) of 0.7 nm and low leakage current (10^{-6} A/cm^2) at -1 V.[25] However, the relatively high D_{it} ($\sim 10^{13}$ eV^{-1}cm^{-2}) likely contributed to the poor mobility of the SHO/Si field-effect transistors (FETs), where both *n*-FETs and *p*-FETs exhibited carrier mobilities of $\sim$25 cm^2/V-s at 1 MV/cm.[25] Later work showed

[a)]Author to whom correspondence should be addressed. Electronic mail: ekerdt@utexas.edu

[This article is copyrighted as indicated in the article. Reuse of AIP content is subject to the terms at: http://scitation.aip.org/termsconditions. Downloaded to] IP: 149.169.223.129 On: Thu, 22 Oct 2015 20:07:53

that the SHO films on Si lacked significant strain and confirmed the in-plane misalignment of grains, which can degrade mobility.[30] The large lattice mismatch between SHO and Si, and subsequent relaxation of the film, likely contributed to the formation of these undesirable defects.

For epitaxial $SrHfO_3$ thin films, Ge is a more suitable substrate than Si in terms of the lattice match. Cubic SHO has a lattice constant of 4.069 Å.[33] The Ge (001) surface has an in-plane atomic spacing of 3.992 Å, which would lead to compressive lattice strain in commensurate, epitaxial SHO films of 1.9%. In addition to the closer lattice match, other physical properties make crystalline SHO a good candidate dielectric for Ge-based devices. Polycrystalline SHO films are reported to have a dielectric constant up to $k \sim 35$,[24,28] leading to an EOT of less than 0.6 nm with a 5 nm film using the ratio of $k/3.9$. However, other studies have reported lower dielectric constants ($k \sim 20$) for SHO,[26,32] similar to the binary oxide HfO_2. Finally, SHO has a large band gap of 6.1 eV with favorable conduction band offset (~2.2 eV) and valence band offset (~3.2 eV) with Ge.[26,34] This is in contrast with Ti-based perovskites, where the Ti 3*d* states yield negligible conduction band offsets with Si and Ge (~0.1–0.5 eV).[21,22,35] A direct comparison between SHO and STO films on Si (001) has shown a reduction in gate leakage by 4 orders of magnitude for SHO versus STO.[26]

Recently, we reported the growth of single crystal STO ($a = 3.905$ Å) on Ge (001) by atomic layer deposition (ALD) followed by post-deposition annealing in vacuum.[23] Capacitor structures revealed a large dielectric constant ($k \sim 90$) for the STO films, but a high leakage current of ~ 10 A/cm^2 for an applied field of 0.7 MV/cm. To circumvent this leakage issue, we explore the Hf-based perovskite, SHO, with optimal band alignments to Ge and associated reduction in leakage current. As detailed in our previous report,[23] the controlled growth by ALD on a clean Ge (001) surface enables a chemical route to epitaxial oxide integration with semiconductors. Here, we confirm this growth and annealing protocol to realize crystalline SHO films, and evaluate the potential for epitaxial SHO films as a future gate dielectric for Ge-based transistors.

II. EXPERIMENTAL

Strontium hafnate, $SrHfO_3$ (SHO), thin films are deposited by ALD at a substrate temperature of 225 °C using strontium bis(triisopropylcyclopentadienyl) [$Sr(^iPr_3Cp)_2$] (HyperSr),[36] hafnium formamidinate (Hf-FAMD),[37] and purified water as co-reactants. Both the Sr and Hf metalorganic precursors are commercially available, reactive with water, and have been previously used for ALD.[38–48] Alternating subcycles of Sr and Hf are used to deposit stoichiometric to slightly Sr-rich (56%) films. During each subcycle the metalorganic is dosed for 2 s to ensure complete saturation of the surface, and subsequently purged for 15 s with ultrahigh purity Ar. The water co-reactant is dosed for 1 s followed by a 15 s Ar purge.

The Ge (001) substrate is prepared from a 4-inch Ge wafer (Sb-doped, $\rho \sim 0.04$ Ω cm) from MTI Corp. The as-received Ge wafer is diced into approximately 18×20 mm^2 sample pieces. The sample is degreased by placing the wafer in ultrasonic baths of acetone, isopropyl alcohol, and water for 10 min each. The sample is then dried with nitrogen and exposed to ultraviolet/ozone for 30 min to remove residual carbon contamination. The sample is then immediately loaded into the load lock chamber and pumped by a turbomolecular pump to a vacuum below 5×10^{-7} Torr before transferring into the annealing chamber. The surface GeO_2 is removed by annealing the sample at 700 °C in vacuum ($<2 \times 10^{-9}$ Torr) for 1 hr. After thermal deoxidation, the Ge substrate is brought to below 200 °C before transfer into the ALD system. The heating and cooling rates are fixed at 20 °C min^{-1}. The low base pressure of the annealing chamber minimizes potential contamination of the Ge surface during thermal deoxidation. The clean Ge (001) surface then shows a sharp, intense 2×1 reconstruction that is observed by *in situ* reflection high-energy electron diffraction (RHEED).

After achieving the 2×1 reconstructed Ge surface, the sample is transferred into the ALD chamber, with a base pressure of 5×10^{-7} Torr, and allowed at least 30 min to reach thermal equilibrium. Ultrahigh purity argon is used as the carrier/purge gas and maintains the deposition pressure at 1.0 Torr. To deposit stoichiometric to Sr-rich (~56%) films of SHO, a subcycle ratio of 1:1 (Sr:Hf) is used. This is in contrast to STO films, where the initial deposition on Ge required a Sr-heavy subcycle ratio of 2:1 (Sr:Ti).[23] Upon deposition of the SHO film, the sample is transferred back into the annealing chamber for crystallization. Post-deposition annealing is carried in vacuum ($<2 \times 10^{-9}$ Torr) with a temperature ramp rate of 20 °C/min.

The SHO films were post-deposition annealed at a substrate temperature of 650–850 °C. The transition of the films from amorphous to crystalline is observed in real time by *in situ* RHEED. After crystallization, *in situ* x-ray photoelectron spectroscopy (XPS) is used to check the chemical composition and oxidation states, as well as to measure the valance band offset of the SHO-Ge heterostructure. XPS is performed using a VG Scienta R3000 analyzer and a monochromated Al Kα source at 1486.6 eV. The analyzer is calibrated using a silver foil, where the Ag $3d_{5/2}$ core level is defined to be 368.28 eV and the Fermi level of Ag at 0.00 eV. High-resolution spectra of Sr (3*d*, 3*p*), Hf (4*f*, $4d_{5/2}$), O 1*s*, C 1*s*, and Ge (3*d*, $2p_{3/2}$) core levels are measured using a pass energy of 100 eV with an analyzer slit width of 0.4 mm, resulting in an effective resolution of 350 meV. Each high-resolution scan is measured four times and summed, using 50 meV steps with a dwell time of 157 ms per step. Film composition is estimated using CasaXPS (version 2.3.16) peak fitting with a Shirley background subtraction and relevant sensitivity factors.[49]

The epitaxial SHO films are characterized *ex situ* by x-ray reflectivity (XRR), x-ray diffraction (XRD), and cross-section transmission electron microscopy (TEM). XRR is performed using a Rigaku Ultima IV equipped for thin-films with automated alignment. XRD is performed using an X'PERT Powder Diffractometer with a sealed tube Cu Kα radiation ($\lambda \sim 1.5406$ Å). Cross-sectional TEM is performed with a 400-keV high-resolution electron microscope (JEM-

[This article is copyrighted as indicated in the article. Reuse of AIP content is subject to the terms at: http://scitation.aip.org/termsconditions. Downloaded to] IP: 149.169.223.129 On: Thu, 22 Oct 2015 20:07:53

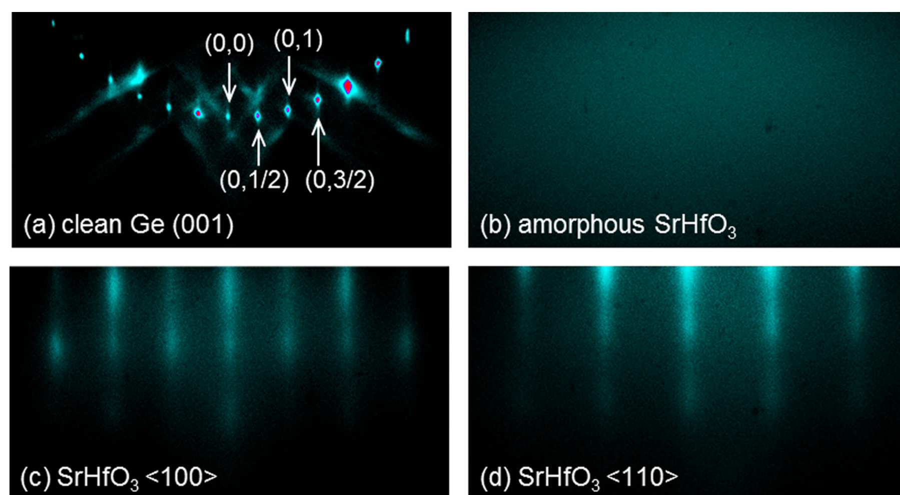

FIG. 1. RHEED patterns for a 2-nm-thick $SrHfO_3$ deposition (a) after thermal deoxidation of the Ge (001) substrate showing a visible 2×1 reconstructed surface, (b) the amorphous $SrHfO_3$ film after ALD and the crystalline SHO film after post-deposition vacuum annealing at 700 °C for 5 min where the beam is aligned along the (c) $\langle 100 \rangle$ and (d) $\langle 110 \rangle$ directions of $SrHfO_3$.

4000EX) equipped with a double-tilt specimen holder. The samples are prepared using standard mechanical polishing followed by argon-ion-milling to perforation.

Standard metal-oxide-semiconductor capacitor (MOSCAP) structures are created for capacitance-voltage (C-V) and current-voltage (I-V) measurements. The top electrode on the oxide surface is formed using sputtering of TaN, photolithography, and SF_6-based plasma etching. The bottom electrode is formed by using silver paste on the scratched backside of the Ge substrate. Both C-V and I-V were measured in air at room temperature under dark conditions using an Agilent B1500A semiconductor device parameter analyzer with a Cascade Microtech probe station. The sweeping voltage was applied to the top electrode with the bottom electrode grounded. The density of interface traps (D_{it}) was estimated using the conductance method with a range of frequencies extending from 1 kHz to 1.2 MHz.[50]

III. RESULTS AND DISCUSSION

A. Deposition and crystallization of $SrHfO_3$ on Ge

Strontium hafnate films were deposited by ALD on the reconstructed Ge (001) at 225 °C. Film thicknesses between 1 and 20 nm were deposited, and the films were subsequently crystallized in vacuum at temperatures greater than 650 °C (typically 700 °C). Some thicker SHO films (>5 nm) were grown in a two-step growth and anneal process for comparison. Figure 1 shows a series of RHEED images for a 2-nm-thick SHO deposition: (a) after thermal deoxidation of the Ge (001) substrate showing a clear 2×1 reconstructed surface and (b) the amorphous SHO film after ALD and the crystalline SHO film after post-deposition vacuum annealing at 700 °C for 5 min, where the beam is aligned along the (c) $\langle 100 \rangle$ and (d) $\langle 110 \rangle$ directions of the perovskite oxide. Four-fold symmetry of the crystalline SHO film was observed by rotating the sample under electron illumination.

In situ XPS analysis was used to check the SHO film stoichiometry. High-resolution scans of the most prominent core-levels, Sr 3*d* and Hf 4*f*, were used for compositional analysis. Representative core-level spectra for a 2-nm-thick SHO film are shown in Figure 2. Both the Sr 3*d* and Hf 4*f* chemical shifts shown in Figs. 2(a) and 2(b), respectively, are consistent with the fully oxidized species ($SrHfO_3$). The fitted peak positions are located at binding energies of 134.0 eV and 135.7 eV for Sr $3d_{5/2}$ and Sr $3d_{3/2}$, respectively, and 16.9 eV and 18.5 eV for Hf $4f_{7/2}$ and Hf $4f_{5/2}$, respectively. The asymmetry observed on the high binding energy side of the Hf 4*f* high-resolution scan is due to overlap of the Sr 4*p* peak, at approximately 19.8 eV. Deconvolution of the spectra allows for subtraction of the Sr 4*p* component and appropriate estimation of the film stoichiometry. For the sample shown in Fig. 2, the Sr:Hf ratio is 56:44. For the growth of crystalline perovskite oxides, stoichiometric to slightly Sr-rich is preferred due to the relative ease with which additional SrO layers can be incorporated while maintaining the film crystallinity. Previous work from our group has shown that Sr-rich STO films maintain the perovskite structure, while Ti-rich STO films are more likely to be amorphous.[46] The samples grown for this study varied slightly in cation stoichiometry from 52% to 56% Sr.

XRD and rocking curve analyses were performed *ex situ* to verify the crystalline structure and out-of-plane alignment, as shown in Figure 3. Fig. 3(a) shows a rocking curve around the SHO (002) peak for a 4.6-nm-thick SHO film, with a full-width half-maximum of 1.2°. The SHO film was post-deposition annealed in vacuum at a substrate temperature of 725 °C for 5 min. Fig. 3(b) shows a schematic model of the cubic perovskite $SrHfO_3$, where the bulk lattice constant is 4.069 Å. Fig. 3(c) shows a θ-2θ scan of the 4.6 nm SHO film

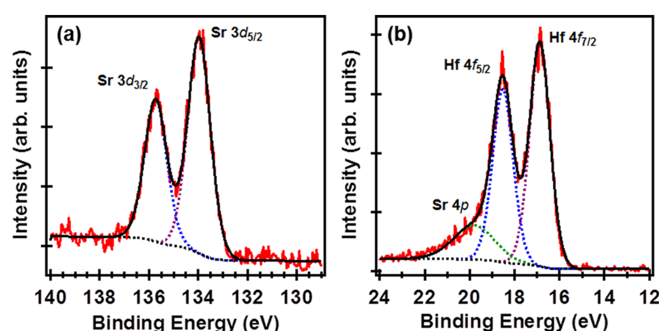

FIG. 2. X-ray photoelectron spectra of a 2-nm-thick $SrHfO_3$ film showing the most prominent core-levels: (a) Sr 3*d* and (b) Hf 4*f*. Deconvolution of the spectra (dashed lines) highlights the individual contributions of the Sr and Hf core-levels to the overall intensity.

[This article is copyrighted as indicated in the article. Reuse of AIP content is subject to the terms at: http://scitation.aip.org/termsconditions. Downloaded to] IP: 149.169.223.129 On: Thu, 22 Oct 2015 20:07:53

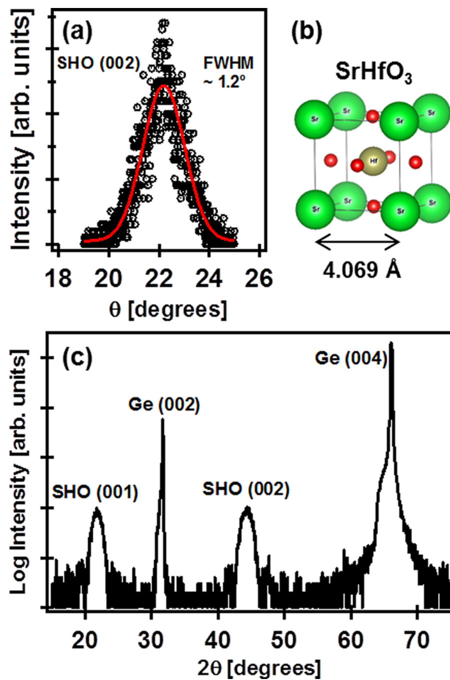

FIG. 3. X-ray diffraction and rocking curve analysis of a 4.6-nm $SrHfO_3$ film on Ge: (a) rocking curve around the SHO (002) peak, with a full-width half-maximum of 1.2°, (b) schematic model of the cubic perovskite $SrHfO_3$ ($a \sim 4.069$ Å), and (c) θ-2θ scan of the 4.6-nm SHO film on Ge, where only (001)-oriented peaks are present.

on Ge, where only the (001)-oriented peaks are present. The SHO (002) peak position, $44.35 \pm 0.05°$, corresponds to an experimental c-axis lattice spacing of 4.082 ± 0.005 Å for the epitaxial film. This suggests that the c-axis is slightly expanded from the bulk, consistent with compressive in-plane strain. Assuming SHO ($a \sim 4.069$ Å) is perfectly strained to the Ge surface (3.992 Å), and a Poisson ratio of 0.25,[51] the expected out-of-plane lattice spacing would be 4.088 Å. This suggests that the 4.6 nm SHO film is at least partially strained to the underlying Ge substrate for the growth and annealing conditions.

B. Band offset of the $SrHfO_3$-Ge heterojunction

In situ XPS analysis was used to estimate the band offset of the SHO-Ge heterojunction. Shallow core-level and valence band spectra were collected for bulk Ge (001), 11.2-nm-thick SHO (001) film grown by ALD, and the SHO-Ge (001) heterojunction. The thick SHO film was grown in a two-step growth and anneal process, with a measured stoichiometric ratio of 54:46 (Sr:Hf). The Ge substrate was prepared by solvent degreasing, UV/ozone exposure, and UHV annealing (700 °C for 1 h) as described in Sec. II. Both core-level and valence band spectra were collected using a monochromated Al Kα source at 1486.6 eV. The valence band spectra for both the clean Ge (001) substrate and the 11.2-nm-thick SHO film are shown in Figure 4.

For the Ge (001) substrate, the energy difference between the valence band edge and Ge $3d_{5/2}$ centroid was 29.30 ± 0.05 eV. For the 11.2-nm-thick SHO film, the energy difference between the valence band edge and the Hf $4f_{7/2}$ centroid was 13.26 ± 0.05 eV. To probe the SHO-Ge heterojunction, a thin ($\sim$2 nm) epitaxial SHO film was grown on Ge. Both the Ge $3d$ and Hf $4f$ core-levels were measured, where the energy difference between the Ge $3d_{5/2}$ and Hf $4f_{7/2}$ centroids was 12.77 ± 0.05 eV. Using the measured energy differences, the valence band offset (VBO) between SHO and Ge was estimated to be -3.27 ± 0.10 eV.

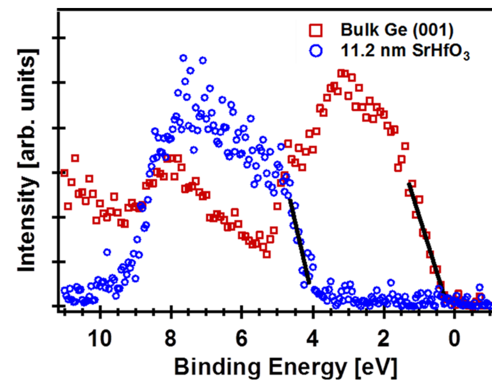

FIG. 4. Valence band spectra for both clean Ge (001) substrate (red squares) and 11.2-nm-thick $SrHfO_3$ film (blue circles).

To calculate the conduction band offset (CBO), we assume the bulk band gap values of SHO and Ge to be 6.1 eV and 0.66 eV, respectively.[26,52] The resulting CBO is 2.17 ± 0.10 eV, as shown schematically in Figure 5. The positive band offset value means the band energy is higher in the epitaxial SHO film. It should be noted, however, that the CBO may be overestimated due to the uncertainty in the bulk SHO band gap value. In other work, the electronic band gap for SHO has been reported to be 5.8 eV based on photoemission spectra and x-ray absorption data.[31] Regardless, the band alignment between crystalline SHO and Ge (001) is well above the minimum $\sim$1 eV band offset required for suitable gate dielectrics.[53]

C. MOSCAP performance

Capacitor structures were made on five samples of varying SHO thickness to measure the capacitance of the oxide

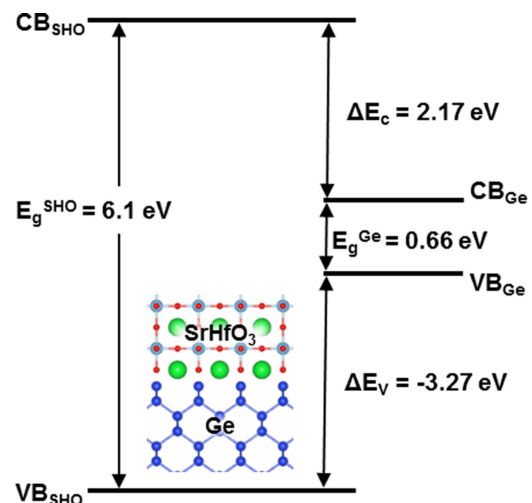

FIG. 5. Band alignment of the SHO-Ge heterojunction estimated using shallow core-level and valence band spectra. The bulk band gap values of SHO and Ge were taken to be 6.1 eV and 0.66 eV, resulting in a CBO of 2.17 eV and VBO of -3.27 eV.

[This article is copyrighted as indicated in the article. Reuse of AIP content is subject to the terms at: http://scitation.aip.org/termsconditions. Downloaded to] IP: 149.169.223.129 On: Thu, 22 Oct 2015 20:07:53

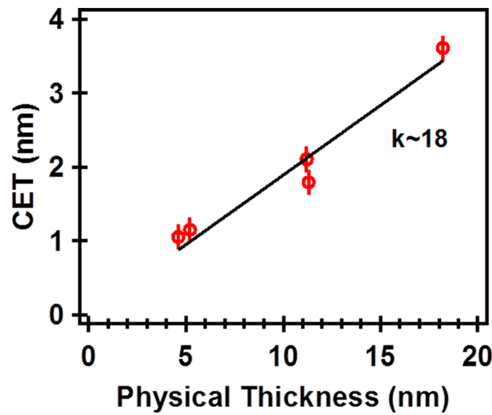

FIG. 6. Plot of CET versus physical thickness for extraction of the dielectric constant for epitaxial $SrHfO_3$ layers grown directly on Ge by atomic layer deposition. The films were crystallized by post-deposition vacuum anneal at 700 °C for 5 min.

layer (C_{ox}) and extract the dielectric constant. These data are summarized in Figure 6 as a plot of capacitance equivalent thickness (CET) versus physical thickness of the epitaxial SHO layer. The dielectric constant is estimated to be $k \sim 18$ for crystalline SHO. This value is much lower than the $k \sim 35$ that was reported previously for polycrystalline SHO grown on TiN/Si substrates by MBE;[24,28] however, it is consistent with lower values reported for epitaxial SHO on Si ($k \sim 20$) and polycrystalline SHO grown by plasma-assisted ALD ($k \sim 21$).[26,32] The high dielectric constant ($k \sim 35$) for polycrystalline SHO was only achieved after post-deposition annealing at 800 °C or higher on TiN/Si substrates,[28] possibly resulting in Ti diffusion into the SHO layer. It is therefore reasonable to conclude that the dielectric constant of SHO is similar to that of the binary oxide HfO_2 ($k \sim 20$).

To understand the effect of crystallization on the electrical performance, a comparison was made between crystalline and amorphous SHO films. Both SHO films were grown directly on the 2×1 reconstructed Ge surface with a nominal thickness of 20 nm. The amorphous SHO film was not post-deposition annealed, whereas the crystalline SHO film was post-deposition annealed at 700 °C for 5 min in vacuum. MOSCAP structures were formed for both the crystalline and amorphous SHO samples. The amorphous SHO film showed a much lower saturation capacitance (C_{ox}) than the crystalline SHO film. This results in an effective dielectric constant of $k \sim 12$ for the amorphous SHO and $k \sim 20$ for the crystalline SHO film. However, despite an increase in dielectric constant, the observed D_{it} was significantly higher for the crystalline film. Using the conductance method, the D_{it} was estimated to be $2 \times 10^{12}\,cm^{-2}eV^{-1}$ and $4 \times 10^{13}\,cm^{-2}eV^{-1}$ for the amorphous and crystalline SHO films, respectively. The increase of interface traps for the crystalline film is cause for concern since one of the expected benefits of epitaxial oxide dielectrics is the potential for drastically reduced interface traps. Additional studies are needed to understand the origin of these interface trap states in ALD-grown epitaxial dielectrics on Ge.

MOSCAP structures were used to evaluate the electrical performance of a 4.6-nm-thick SHO film grown on Ge by ALD, where the SHO film is still partially strained to the Ge substrate. The SHO was crystallized with a post-deposition anneal at 725 °C in vacuum for 5 min. Both C-V and I-V measurements were performed on a 15-μm radius top electrode. The C-V and I-V curves for the 4.6-nm SHO on Ge are shown in Figure 7, where the capacitance and current are normalized by the area of the top electrode. Fig. 7(a) shows the C-V and I-V response of the 4.6-nm-thick SHO film after removal from the UHV system, where the C-V is taken at a frequency of 1 MHz. C_{ox} saturates at $\sim 3.3\ \mu F/cm^2$ under accumulation, yielding a dielectric constant of $k \sim 17$ for the SHO film. The 4.6-nm-thick SHO film shows a low leakage current of $6.3 \times 10^{-6}\ A/cm^2$ for an applied electric field of 1 MV/cm with an EOT of ~ 1.0 nm. This corresponds to a reduction of over seven orders of magnitude in leakage current when compared with a 15-nm-thick STO film on Ge.[23] The massive reduction in leakage current is attributed to the favorable conduction band offset (2.2 eV) for SHO on Ge; whereas, STO shows negligible conduction band offset (0.1 eV) under similar measurement conditions.[23]

Using the conductance method, D_{it} was estimated to be $1 \times 10^{13}\,cm^{-2}eV^{-1}$. This relatively high D_{it} may result from an interfacial reaction that occurs during the vacuum anneal for crystallization of the SHO layer. This reaction is studied in detail in Sec. III D. In efforts to reduce D_{it}, the 4.6-nm-thick SHO was post-deposition air annealed at 300 °C for 30 min after removal from the UHV system. Fig. 7(b) shows the C-V and I-V response of the SHO film after air anneal. The C-V response at a frequency of 1 MHz shows the emergence of a bump in the weak inversion region (~ -0.2 V) after air anneal that was not observed in the as-deposited sample. The exact origin of this defect state is not yet known. C_{ox} saturates at $\sim 3.1\ \mu F/cm^2$ under accumulation, indicating minimal change

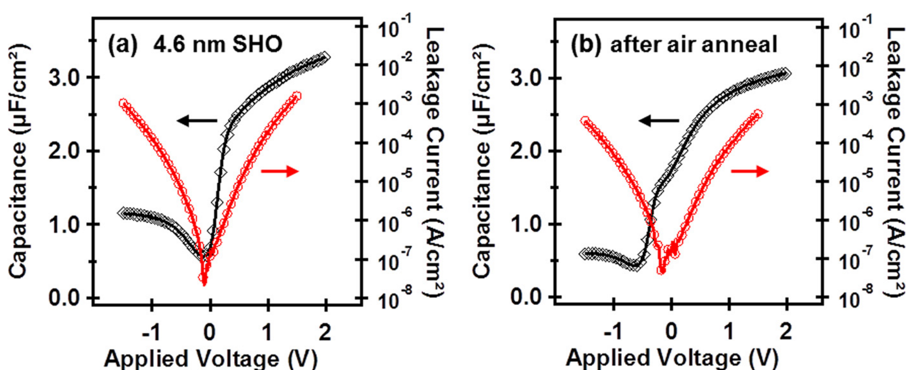

FIG. 7. Capacitance-voltage (black curves) and current-voltage (red curves) measurements for a 4.6-nm-thick SHO film grown by ALD on Ge. The SHO film was crystallized by a post-deposition vacuum anneal at 725 °C for 5 min. Electrical measurements were taken: (a) before and (b) after, *ex situ* air anneal at 300 °C for 30 min.

[This article is copyrighted as indicated in the article. Reuse of AIP content is subject to the terms at: http://scitation.aip.org/termsconditions. Downloaded to] IP: 149.169.223.129 On: Thu, 22 Oct 2015 20:07:53

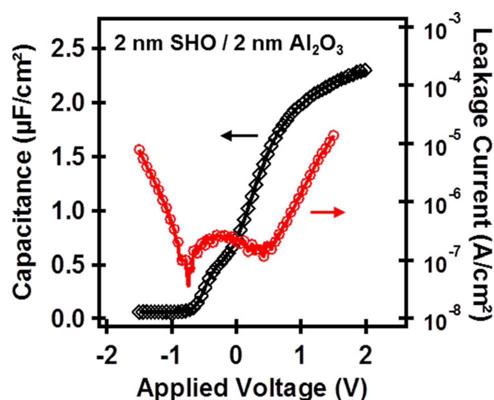

FIG. 8. Capacitance-voltage (black curve) and current-voltage (red curve) measurements for 2-nm-thick SHO film on Ge with a 2-nm-thick Al_2O_3 capping layer. The SHO film was crystallized by a post-deposition vacuum anneal at 650 °C for 5 min before depositing the amorphous Al_2O_3 capping layer.

in the dielectric constant ($k \sim 16$). The leakage current is slightly improved to 4.0×10^{-6} A/cm^2 for an applied electric field of 1 MV/cm with an EOT of ~1.1 nm. The D_{it} for the air annealed sample was reduced to $6 \times 10^{12}\,\mathrm{cm}^{-2}\,\mathrm{eV}^{-1}$.

For comparison, the electrical performance of 2-nm-thick crystalline SHO with a 2-nm-thick Al_2O_3 capping layer was evaluated. The 2-nm-thick SHO film was crystallized at a relatively lower temperature of 650 °C, leading to a more abrupt interface, as discussed in Sec. III D. The Al_2O_3 capping layer was needed to prevent excess leakage current through the thin SHO layer. With this dielectric stack, the crystalline SHO layer is used to minimize D_{it} at the oxide-Ge interface and the amorphous Al_2O_3 is an excellent leakage barrier. Figure 8 shows the C-V and I-V response of the SHO/Al_2O_3 dielectric stack on Ge after air annealing at 300 °C for 30 min. The SHO/Al_2O_3 stack has a very low leakage current of 1.9×10^{-7} A/cm^2 for an applied electric field of 1 MV/cm with an EOT of ~1.5 nm. As expected, the overall C_{ox} saturates at a lower value (~2.3 μF/cm^2) than the 4.6-nm-thick SHO film. Once again, a small bump is observed in the weak inversion region of the C-V response after air anneal. Assuming a dielectric constant of $k \sim 18$ for the SHO film, the dielectric constant of the Al_2O_3 capping layer is $k \sim 8$. This value is consistent with other reports of Al_2O_3 deposited by ALD with the same co-reactants under similar conditions.[54,55] The D_{it} for the SHO/Al_2O_3 dielectric stack is estimated to be $2 \times 10^{12}\,\mathrm{cm}^{-2}\,\mathrm{eV}^{-1}$. We attribute this lower D_{it} value to the lower annealing temperature (650 °C) required to crystallize the SHO film. More detailed analysis of the electrical performance and origin of defect states in crystalline SHO on Ge will be the subject of future work.

D. Crystallization temperature and the $SrHfO_3$-Ge interface

In all cases, strontium hafnate films deposited by ALD required post-deposition annealing for crystallization; however, the onset of crystallization varied between 650 and 750 °C depending on the thickness of the SHO film. The lowest crystallization temperature observed was at a substrate temperature of 650 °C for a 2-nm-thick SHO film. For very thin (~1 nm) SHO films, the temperature required for crystallization increased to 750 °C due to the substrate retarding crystallization. In all cases, SHO films between 2 and 20-nm-thick appeared fully crystallized when vacuum annealed at a substrate temperature of 700 °C for 5 min. At 700 °C, the temperature is approximately 80% of the Ge melting point (~940 °C), which could lead to interfacial instabilities due to Ge diffusion. In the previous work, interfacial reaction between Ge and Hf metal has been reported to cause formation of a hafnium germanide ($HfGe_2$) at temperatures above ~600 °C.[56]

The effects of annealing temperature on the SHO-Ge heterostructure were examined by *in situ* RHEED and XPS. A very thin (~1 nm) SHO film was used so that the subtle changes in the Ge 3*d* core-level with increasing anneal temperature could be observed. A series of RHEED patterns are shown in Figures 9(a)–9(c). The crystallization of the film can be observed at increasing temperatures of 650, 750, and 850 °C. At the lowest temperature of 650 °C (Fig. 9(a)), the SHO film appears amorphous. The film is thin enough that some electron diffraction is observed from the underlying Ge substrate. After annealing to 750 °C (Fig. 9(b)), the SHO film appears crystalline as shown by the appearance of an ordered streak pattern. The beam is aligned along the ⟨100⟩ direction of the film. When annealed at 850 °C (Fig. 9(c)), the diffraction patterns are more prominent. However, there are additional 1/2-order streaks present that may be due to a secondary phase formation at the interface.

The corresponding series of Ge 3*d* spectra collected by *in situ* XPS shown in Figs. 9(d)–9(f) provide insight into the interfacial reaction that occurs between SHO and Ge. The overall Ge 3*d* signal becomes less defined (broader) with increasing anneal temperature. Deconvolution of the Ge 3*d* core-level in CasaXPS also reveals that spectral components of both lower and higher binding energy than the bulk peak increase with higher temperature annealing. The lower binding energy component is attributed to a combination of "interfacial Ge" and Ge-Hf bonding. The chemical shift ($\Delta\varepsilon = -0.5$ eV) observed for the interfacial Ge component appears similar to Ge (001) surface dimerization.[57] A similar chemical shift (−0.46 eV) is expected for Ge-Hf bonding from first-principles calculations.[58] The percentage of the Ge $3d_{5/2}$ component associated with the lower binding energy relative to the entire Ge signal is shown to increase with temperature. The relative area of this component is 2.2%, 2.7%, and 5.6% for the film annealed at 650 °C, 750 °C, and 850 °C, respectively. We associate the increase in this component with an interfacial reaction between SHO and Ge with increasing temperature, although the small difference in relative area between 650 °C and 750 °C may not be significant. The more substantial change in the relative area of the lower binding energy component at 850 °C is attributed to an increase in Ge-Hf bonding. There is also an increase in the higher binding energy component, which is attributed to Ge^{1+} formation ($\Delta\varepsilon = 0.70$ eV).[59] At higher annealing temeperatures, desorption of the SHO film may occur; however, no noticeable changes in the Sr 3*d* or O 1*s* core-levels were observed after annealing at 850 °C (not shown). Only a slight shift (~0.2 eV) to lower binding energy was observed in the

[This article is copyrighted as indicated in the article. Reuse of AIP content is subject to the terms at: http://scitation.aip.org/termsconditions. Downloaded to] IP: 149.169.223.129 On: Thu, 22 Oct 2015 20:07:53

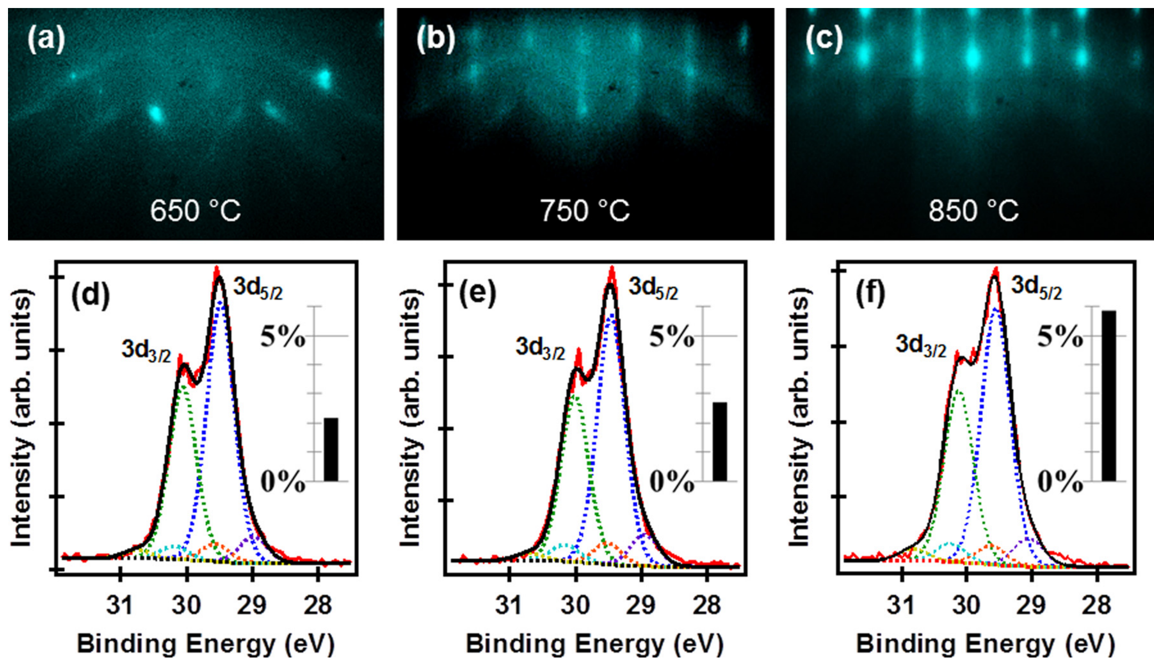

FIG. 9. Effects of annealing temperature on the SHO-Ge heterostructure examined by *in situ* RHEED and XPS. RHEED patterns are shown at increasing anneal temperatures of (a) 650 °C, (b) 750 °C, and (c) 850 °C. The corresponding Ge 3*d* core-level spectra are shown in (d)–(f) for the 650–850 °C anneal temperature, respectively. The extent of interfacial reaction is quantified by the percent of Ge $3d_{5/2}$ for the lower binding energy component relative to the total Ge signal, as shown graphically on the right side of the high-resolution scan.

Hf 4*f* core-level with increased annealing temperature (not shown), which is also attributed to an increase in Ge-Hf bonding.

As further confirmation of an interfacial reaction, the SHO-Ge heterostructure was explored by cross-sectional TEM observations. SHO films were vacuum annealed at 650 °C and 700 °C to compare the abruptness of the SHO-Ge interface. The 2-nm-thick SHO film was post-deposition annealed at 650 °C for 5 min and then capped with 2 nm of amorphous Al_2O_3 before removal from the UHV system. The thicker SHO film (5.2-nm-thick) was annealed at 700 °C and was removed from the system without a capping layer. The 5.2-nm-thick SHO film was grown in a two-step growth and anneal process (2 nm plus 3.2 nm) with post-deposition annealing at 700 °C for 5 min following each growth. Electron micrographs of the two films are compared in Figure 10. At a substrate temperature of 650 °C (Fig. 10(a)), the SHO-Ge interface appears abrupt with a negligible interfacial layer (IL). However, for the higher substrate temperature of 700 °C (Fig. 10(b)), there is a clear presence of an IL at the SHO-Ge interface. The thickness of this IL appears to be ∼0.5 nm, indicating that the interfacial reaction here is limited to 1–2 atomic layers. Regardless, this IL formation appears correlated to higher D_{it} values as discussed Sec. III C. The electron micrographs, along with the XPS analysis, indicate that a low crystallization temperature (<650 °C) is necessary to maintain an abrupt interface for the SHO-Ge heterojunction. An abrupt interface may be necessary to reduce D_{it} for the desired electrical performance of the crystalline oxide on Ge.

With this material system, there is a tradeoff between sufficient thermal energy for crystallization to achieve a higher dielectric constant, while also maintaining a lower temperature to minimize interfacial reactions and D_{it}. As mentioned above, the 2-nm-thick SHO film began crystallizing at the lowest temperature of 650 °C. However, typical SHO films grown by this method crystallized somewhere between 650–700 °C, appearing fully crystalline by RHEED at 700 °C. The obvious concern is that at temperatures below 700 °C, films will not be fully crystallized and suffer from a lower dielectric constant. As a complicating factor, higher anneal temperatures are also correlated with increasing D_{it} values. The lowest D_{it} values for SHO on Ge were measured for films with no post-deposition anneal (amorphous films) or where the post-deposition anneal was kept at or below 650 °C. Low magnification electron micrographs of the two films discussed above are shown in Figure 11. The top image (Fig. 11(a)) reveals that the SHO film annealed at 650 °C has some tiny isolated amorphous regions, as denoted by the

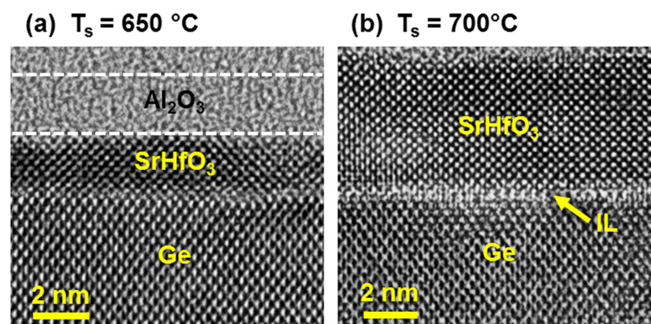

FIG. 10. Transmission electron micrographs of: (a) 2-nm-thick SHO post-deposition annealed at 650 °C for 5 min and then capped with 2 nm of amorphous Al_2O_3 and (b) 5.2-nm-thick SHO film grown in a two-step growth and anneal process (2 nm and 3.2 nm) with post-deposition annealing at 700 °C for 5 min. A higher anneal temperature of 700 °C, results in the formation of a very thin IL at the SHO-Ge interface.

[This article is copyrighted as indicated in the article. Reuse of AIP content is subject to the terms at: http://scitation.aip.org/termsconditions. Downloaded to] IP: 149.169.223.129 On: Thu, 22 Oct 2015 20:07:53

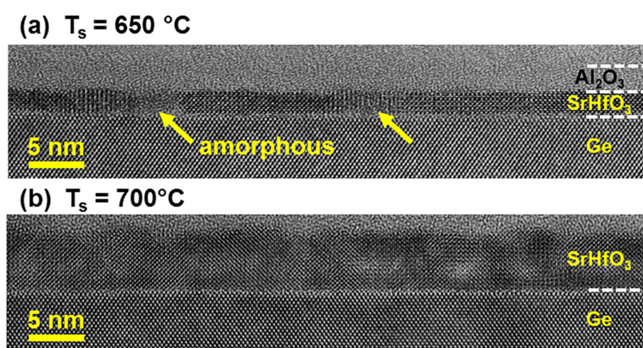

FIG. 11. Low magnification electron micrographs of: (a) 2-nm-thick SHO film post-deposition annealed at 650 °C for 5 min and then capped with 2 nm of amorphous Al_2O_3 and (b) 5.2-nm-thick SHO film grown in a two-step growth and anneal process (2 nm and 3.2 nm) with post-deposition annealing at 700 °C for 5 min. Tiny amorphous regions are visible in (a), attributed to the reduced post-deposition anneal temperature.

arrows. The thicker SHO film annealed at 700 °C, shown in Fig. 11(b), does not show any sign of amorphous regions. In both cases, the SHO films show excellent epitaxial alignment with the Ge substrate, and the deposited films are uniform in thickness. Further study is clearly required to optimize the annealing conditions to achieve high crystallinity to increase the dielectric constant, while maintaining an abrupt interface to minimize interface traps.

IV. CONCLUSIONS

Crystalline strontium hafnate, $SrHfO_3$ (SHO), films have been grown by atomic layer deposition directly on Ge (001) substrates. The 2×1 reconstructed Ge (001) surface was prepared by thermal annealing in vacuum and transferred *in situ* to the ALD system. After deposition of an amorphous SHO layer (~2–20 nm), the film was crystallized by post-deposition anneal (~700 °C) in vacuum. The crystalline SHO films were confirmed to be (001)-oriented with epitaxial registry to the Ge (001) surface. Band offset measurements indicate that the SHO has favorable band offsets with Ge for gate dielectric applications, with a VBO of −3.27 eV and CBO of 2.17 eV. Electrical measurements of MOSCAP structures estimate the dielectric constant of crystalline SHO to be $k \sim 18$. The leakage current of a 4.6-nm-thick SHO film was 6.3×10^{-6} A/cm^2 for an applied electric field of 1 MV/cm, which indicates a significant advantage of Hf-based perovskites over Ti-based perovskites, such as STO. The lowest D_{it} value for the SHO-Ge heterojunction was estimated to be 2×10^{12} cm^{-2}eV^{-1}. Interestingly, D_{it} is not improved by crystallization of the SHO layer and is negatively impacted by higher post-deposition annealing temperature and corresponding abruptness of the SHO-Ge interface. The current work shows extremely promising potential for the integration of crystalline oxides on Ge by atomic layer deposition for advanced electronic applications.

ACKNOWLEDGMENTS

This work was supported by the National Science Foundation (Award Nos. CMMI-1437050 and DMR-1207342), the Office of Naval Research (Grant No. N00014-10-10489), and the Air Force Office of Scientific Research (Grant No. FA9550-12-10494).

[1]K. Rim, R. Anderson, D. Boyd, F. Cardone, K. Chan, H. Chen, S. Christansen, J. Chu, K. Jenkins, T. Kanarsky, S. Koester, B. H. Lee, K. Lee, V. Mazzeo, A. Mocuta, D. Mocuta, P. M. Mooney, P. Oldiges, J. Ott, P. Ronsheim, R. Roy, A. Steegen, M. Yang, H. Zhu, M. Ieong, and H. S. P. Wong, Solid-State Electron. **47**, 1133 (2003).
[2]S. E. Thompson, M. Armstrong, C. Auth, M. Alavi, M. Buehler, R. Chau, S. Cea, T. Ghani, G. Glass, and T. Hoffman, IEEE Trans. Electron. Devices **51**, 1790 (2004).
[3]R. Chau, B. Doyle, S. Datta, J. Kavalieros, and K. Zhang, Nat. Mater. **6**, 810 (2007).
[4]K. C. Saraswat, C. O. Chui, T. Krishnamohan, A. Nayfeh, and P. McIntyre, Microelectron. Eng. **80**, 15 (2005).
[5]D. P. Brunco, B. De Jaeger, G. Eneman, A. Satta, V. Terzieva, L. Souriau, F. E. Leys, G. Pourtois, M. Houssa, K. Opsomer, G. Nicholas, M. Meurius, and M. Heyns, ECS Trans. **11**, 479 (2007).
[6]R. Pillarisetty, Nature **479**, 324 (2011).
[7]S. Gupta, X. Gong, R. Zhang, Y.-C. Yeo, S. Takagi, and K. C. Saraswat, MRS Bull. **39**, 678 (2014).
[8]R. Droopad, K. Eisenbeiser, and A. A. Demkov, in *High Dielectric Constant Materials*, edited by H. R. Huff and D. C. Gilmer (Springer, Berlin, Heidelberg, 2005), Vol. 16, p. 639.
[9]R. A. McKee, F. J. Walker, and M. F. Chisholm, Phys. Rev. Lett. **81**, 3014 (1998).
[10]R. Droopad, Z. Yu, J. Ramdani, L. Hilt, J. Curless, C. Overgaard, J. L. Edwards, Jr., J. Finder, K. Eisenbeiser, and W. Ooms, Mater. Sci. Eng. B **87**, 292 (2001).
[11]R. John, Rep. Prog. Phys. **69**, 327 (2006).
[12]A. A. Demkov, A. B. Posadas, H. Seo, M. Choi, K. J. Kormondy, P. Ponath, R. C. Hatch, M. D. McDaniel, T. Q. Ngo, and J. G. Ekerdt, ECS Trans. **54**, 255 (2013).
[13]C. Claeys and E. Simoen, *Germanium-Based Technologies: From Materials to Devices* (Elsevier Science, 2007).
[14]Y. Kamata, Mater. Today **11**, 30 (2008).
[15]K. Kita, T. Takahashi, H. Nomura, S. Suzuki, T. Nishimura, and A. Toriumi, Appl. Surf. Sci. **254**, 6100 (2008).
[16]M. Caymax, M. Houssa, G. Pourtois, F. Bellenger, K. Martens, A. Delabie, and S. Van Elshocht, Appl. Surf. Sci. **254**, 6094 (2008).
[17]R. M. Wallace, P. C. McIntyre, J. Kim, and Y. Nishi, MRS Bull. **34**, 493 (2009).
[18]I.-K. Oh, M.-K. Kim, J.-S. Lee, C.-W. Lee, C. Lansalot-Matras, W. Noh, J. Park, A. Noori, D. Thompson, S. Chu, W. J. Maeng, and H. Kim, Appl. Surf. Sci. **287**, 349 (2013).
[19]K. D. Fredrickson, P. Ponath, A. B. Posadas, M. R. McCartney, T. Aoki, D. J. Smith, and A. A. Demkov, Appl. Phys. Lett. **104**, 242908 (2014).
[20]R. A. McKee, F. J. Walker, and M. F. Chisholm, Science **293**, 468 (2001).
[21]S. A. Chambers, Y. Liang, Z. Yu, R. Droopad, and J. Ramdani, J. Vac. Sci. Technol. A **19**, 934 (2001).
[22]F. Amy, A. S. Wan, A. Kahn, F. J. Walker, and R. A. McKee, J. Appl. Phys. **96**, 1635 (2004).
[23]M. D. McDaniel, T. Q. Ngo, A. Posadas, C. Hu, S. Lu, D. J. Smith, E. T. Yu, A. A. Demkov, and J. G. Ekerdt, Adv. Mater. Interfaces **1**(8), 1400081 (2014).
[24]I. McCarthy, M. P. Agustin, S. Shamuilia, S. Stemmer, V. V. Afanas'ev, and S. A. Campbell, Thin Solid Films **515**, 2527 (2006).
[25]C. Rossel, B. Mereu, C. Marchiori, D. Caimi, M. Sousa, A. Guiller, H. Siegwart, R. Germann, J. P. Locquet, J. Fompeyrine, D. J. Webb, C. Dieker, and J. W. Seo, Appl. Phys. Lett. **89**, 053506 (2006).
[26]M. Sousa, C. Rossel, C. Marchiori, H. Siegwart, D. Caimi, J.-P. Locquet, D. J. Webb, R. Germann, J. Fompeyrine, K. Babich, J. W. Seo, and C. Dieker, J. Appl. Phys. **102**, 104103 (2007).
[27]C. Rossel, M. Sousa, C. Marchiori, J. Fompeyrine, D. Webb, D. Caimi, B. Mereu, A. Ispas, J. P. Locquet, H. Siegwart, R. Germann, A. Tapponnier, and K. Babich, Microelectron. Eng. **84**, 1869 (2007).
[28]G. Lupina, G. Kozłowski, J. Dabrowski, P. Dudek, G. Lippert, and H.-J. MussigMussig, Appl. Phys. Lett. **93**, 252907 (2008).
[29]G. Łupina, O. Seifarth, G. Kozłowski, P. Dudek, J. Dąbrowski, G. Lippert, and H. J. Müssig, Microelectron. Eng. **86**, 1842 (2009).
[30]M. Sawkar-Mathur, C. Marchiori, J. Fompeyrine, M. F. Toney, J. Bargar, and J. P. Chang, Thin Solid Films **518**, S118 (2010).

[This article is copyrighted as indicated in the article. Reuse of AIP content is subject to the terms at: http://scitation.aip.org/termsconditions. Downloaded to] IP: 149.169.223.129 On: Thu, 22 Oct 2015 20:07:53

[31]G. Lupina, O. Seifarth, P. Dudek, G. Kozlowski, J. Dabrowski, H.-J. Thieme, G. Lippert, T. Schroeder, and H.-J. Müssig, Phys. Status Solidi B **248**, 323 (2011).
[32]K. Black, M. Werner, R. Rowlands–Jones, P. R. Chalker, and M. J. Rosseinsky, Chem. Mater. **23**, 2518 (2011).
[33]A. S. Verma and V. K. Jindal, J. Alloys Compd. **485**, 514 (2009).
[34]L. Bjaalie, B. Himmetoglu, L. Weston, A. Janotti, and C. G. Van de Walle, New J. Phys. **16**, 025005 (2014).
[35]X. Zhang, A. A. Demkov, H. Li, X. Hu, Y. Wei, and J. Kulik, Phys. Rev. B **68**, 125323 (2003).
[36]Manufactured and supplied by Air Liquide ALOHA Electronics Performance Materials, Air Liquide Electronics U.S. LP, Houston, TX.
[37]Manufactured and supplied by Dow Electronic Materials, The Dow Chemical Company, North Andover, MA.
[38]M. Vehkamäki, T. Hatanpää, T. Hänninen, M. Ritala, and M. Leskelä, Electrochem. Solid-State Lett. **2**, 504 (1999).
[39]M. Vehkamäki, T. Hänninen, M. Ritala, M. Leskelä, T. Sajavaara, E. Rauhala, and J. Keinonen, Chem. Vap. Deposition **7**, 75 (2001).
[40]R. Katamreddy, V. Omarjee, B. Feist, C. Dussarrat, M. Singh, and C. Takoudis, ECS Trans. **16**, 487 (2008).
[41]R. Katamreddy, Z. Wang, V. Omarjee, P. V. Rao, C. Dussarrat, and N. Blasco, ECS Trans. **25**, 217 (2009).
[42]B. Willis and C. B. Zhang, ECS Trans. **33**, 51 (2010).
[43]C. B. Zhang, L. Wielunski, and B. G. Willis, Appl. Surf. Sci. **257**, 4826 (2011).
[44]S. W. Lee, J. H. Han, S. Han, W. Lee, J. H. Jang, M. Seo, S. K. Kim, C. Dussarrat, J. Gatineau, Y.-S. Min, and C. S. Hwang, Chem. Mater. **23**, 2227 (2011).
[45]W. Lee, J. H. Han, W. Jeon, Y. W. Yoo, S. W. Lee, S. K. Kim, C.-H. Ko, C. Lansalot-Matras, and C. S. Hwang, Chem. Mater. **25**, 953 (2013).
[46]M. D. McDaniel, A. Posadas, T. Q. Ngo, A. Dhamdhere, D. J. Smith, A. A. Demkov, and J. G. Ekerdt, J. Vac. Sci. Technol. A **31**, 01A136 (2013).
[47]M. D. McDaniel, A. Posadas, T. Q. Ngo, C. M. Karako, J. Bruley, M. M. Frank, V. Narayanan, A. A. Demkov, and J. G. Ekerdt, J. Appl. Phys. **115**, 224108 (2014).
[48]H. Li and D. V. Shenai, *Symposium C - CMOS Gate-Stack Scaling-Materials, Interfaces and Reliability Implications* (Mater. Res. Soc. Symp. Proc., 2009), Vol. 1155, p. C04.
[49]C. D. Wagner, J. Electron. Spectrosc. Relat. Phenom. **32**, 99 (1983).
[50]K. Martens, C. O. Chui, G. Brammertz, B. De Jaeger, D. Kuzum, M. Meuris, M. M. Heyns, T. Krishnamohan, K. Saraswat, H. E. Maes, and G. Groeseneken, IEEE Trans. Electron. Devices **55**, 547 (2008).
[51]S. Yamanaka, T. Maekawa, H. Muta, T. Matsuda, S.-i. Kobayashi, and K. Kurosaki, J. Alloys Compd. **381**, 295 (2004).
[52]O. Madelung, *Semiconductors-Data Handbook* (Springer, 2004).
[53]D. G. Schlom, S. Guha, and S. Datta, MRS Bull. **33**, 1017 (2008).
[54]M. D. Groner, J. W. Elam, F. H. Fabreguette, and S. M. George, Thin Solid Films **413**, 186 (2002).
[55]M. D. Groner, F. H. Fabreguette, J. W. Elam, and S. M. George, Chem. Mater. **16**, 639 (2004).
[56]S. Gaudet, C. Detavernier, A. J. Kellock, P. Desjardins, and C. Lavoie, J. Vac. Sci. Technol. A **24**, 474 (2006).
[57]P. E. J. Eriksson and R. I. G. Uhrberg, Phys. Rev. B **81**, 125443 (2010).
[58]G. Pourtois, M. Houssa, A. Delabie, T. Conard, M. Caymax, M. Meuris, and M. M. Heyns, Appl. Phys. Lett. **92**, 032105 (2008).
[59]A. Molle, M. N. K. Bhuiyan, G. Tallarida, and M. Fanciulli, Appl. Phys. Lett. **89**, 083504 (2006).

[This article is copyrighted as indicated in the article. Reuse of AIP content is subject to the terms at: http://scitation.aip.org/termsconditions. Downloaded to] IP: 149.169.223.129 On: Thu, 22 Oct 2015 20:07:53